Available online at www.sciencedirect.com

ScienceDirect

Procedia Engineering 4 (2010) 273–281

Procedia Engineering

www.elsevier.com/locate/procedia

ISAB-2010

Numerical analysis of interfacial shear degradation effects on axial uplift bearing capacity of a tension pile

Wenjie Yan, Fuping Gao*

Key Laboratory for Hydrodynamics and Ocean Engineering, Institute of Mechanics, Chinese Academy of Sciences, Beijing 100190, China

Received 15 July 2010; revised 31 July 2010; accepted 1 August 2010

Abstract

The bearing capacity of tension piles involves complex interactions between the tension-pile with the neighboring sediments. A two-dimensional axisymmetric finite element model (FEM) is proposed and verified with the existing experimental results to simulate the uplift resistance of the pile under axial/vertical loading. With an updated contact-pair algorithm for modeling pile-soil interfacial behavior, the modeling for both the interfacial bonding and the sliding friction mechanisms is fulfilled in the present model, which is capable of simulating the shear degradation effects by the breakage treatment of the pile-soil bonding. The bearing capacity of tension piles in various sediments can be predicted efficiently. Numerical results indicate that, due to the interfacial bonding effect, the enhancement of the tension bearing capacity gets more obvious for higher cohesion strength of the sediments. The interfacial bonding degradation of is the main reason for the occurrence of "critical embedded length" phenomenon.

Keywords: tension pile; pile-soil interaction; bearing capacity; interfacial bonding effects

1. Introduction

Tension pile foundations are widely used in the geotechnical engineering to sustain uplift load from the superstructure, such as offshore floating platforms, submerged floating tunnel, etc. In the past few decades, quite a few studies have been conducted to investigate the capacity of tension pile foundations, but the design of tension pile foundations still needs much empirical treatment [1].

The bearing capacities of tension piles are governed by the complex pile-sediment/soil interaction behavior. There usually exist two pile-sediment interaction mechanisms, i.e. the friction mechanism and the bonding mechanism. For a frictional tension pile, the lateral resistance q_{u} may be expressed as $q_u = \mu_s \sigma_n$, where μ_{s} is the coefficient of sliding friction; σ_n is the interfacial normal stress. Then tension capacity can be deduced with the

* Corresponding author. Tel.: +86-10-82544189; fax: +86-10-82543663.
E-mail address: fpgao@imech.ac.cn

1877-7058 © 2010 Published by Elsevier Ltd. Open access under CC BY-NC-ND license.
doi:10.1016/j.proeng.2010.08.031

frictional resistance, though few engineering properties of pile or soil are concerned in this equation. Modifications for the frictional resistance have been made with respect to the difference between the theoretical results and the field test data. By modifying the coefficient of earth pressure, Meyerhof & Adams [2] proposed an updated formula, which became more consistent with the experiment results. The experiments showed that, the increase of the pile uplift resistance with the embedment is relatively smaller, so Das [3] suggested that the tension capacity should be calculated separately for different embedment depth. The effect of soil failure configuration on the bearing capacity was taken into account in the method proposed by Chattopadhyay & Pise [4].

For the in-situ bored tension-piles, the pile-soil bonding effects become much more crucial to the bearing capacity, especially for the design of rock-socketed bolts. In such case, the side resistance is relevant to both uniaxial strength of the rock σ_c and the compression strength of the grout material f_c. For the ultimate limit state, empirical values of q_u can be set as $0.05\sigma_c \sim 0.4\sigma_c$, if σ_c is relatively small [5-7]; otherwise, q_u is approximately equal to $0.05 f_c$ [8].

The shear stress degradation with the increase of shear strain is a significant characteristic of the interfacial bonding effects, which has been observed in the experiments [9-10]. For a tension pile embedded into rocks, there may exist both the bonding effect and the friction effect. Based on the experimental data, Costamagna *et al*. [11] proposed a failure criterion, in which both the interfacial friction and the fracture of rocks are taken into account. For the simplicity, the Coulomb Friction model can be used to describe the aforementioned two interfacial mechanisms [12]:

$$q_u = c_b + \mu_s \sigma_n \tag{1}$$

where c_b is the interfacial bonding strength. When the tangent strain gets large enough, the bonding would collapse, and the residual sliding resistance degrades into

$$q_{res} = \mu_s \sigma_n \tag{2}$$

The degradation process of lateral resistance has become increasingly attractive. Several theoretical analyses for bolts or piles embedded in rocks have been proposed [13-15].

In this paper, a two-dimensional axisymmetric FEM model is proposed to simulate the pile-sediment interaction under axial/vertical loading. Both the bonding mechanism and the frictional mechanism are taken into account in the numerical model, and the influence of the pile-soil interfacial behavior to the uplift resistance capacity is investigated.

2. Numerical modeling of tension pile-sediment interaction: An axisymmetric model

The bearing process of a single cylindrical pile under an axial uplift load can be considered as an axisymmetric problem (see Fig. 1(a)). A two-dimensional axisymmetric Finite Element Model (FEM) is thereby proposed for simulating the tension pile-soil interaction. The bearing capacity of the vertical loaded tension pipe is further investigated.

2.1. Finite element mesh

Fig. 1(b) illustrates the geometry of the finite element model, which is mainly consisted of the tension pile and the surrounding sediments. Both the pile and sediment are composed with 4-node reduced-integration axisymmetric solid elements provided by ABAQUS software [16]. In the finite element model, the number of the quad elements is approximately in the range of $2\times10^4 \sim 7\times10^4$. The computational grids get denser in the closer proximity to the pile for a reasonable computation efficiency, whose spacing sensitivity has been examined for different pile diameter.

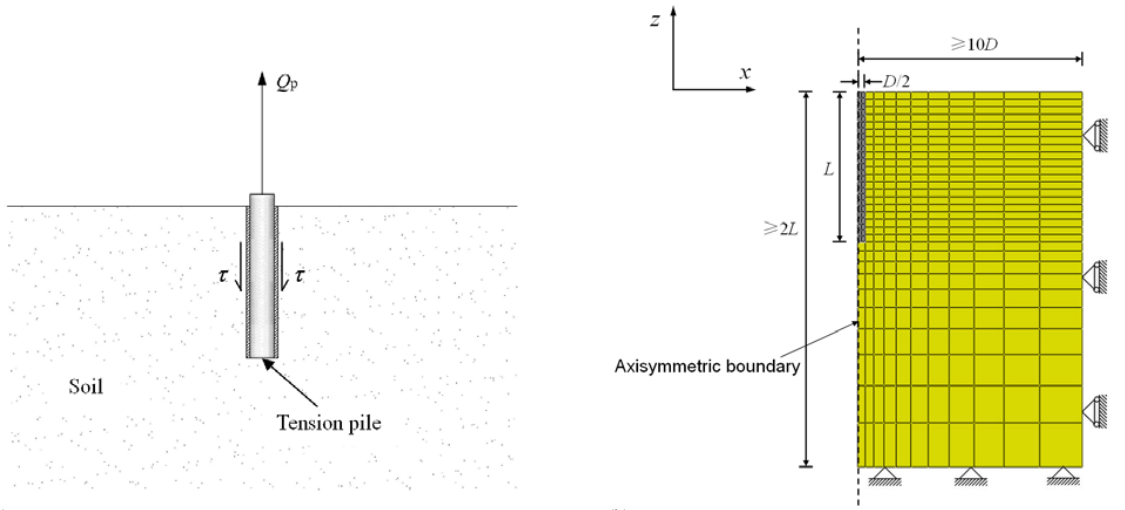

Fig. 1. (a) An illustration of a tension pile under axial loading; (b) Sketch for the computational mesh (not in scale) and the boundary conditions

2.2. Constitutive models of materials

A linear elastic constitutive model is adopted for the tension pile, since the failure of the pile structure usually does not occur during the loading process in the field. As for the sediments of the stratum, their plasticity characteristics may result in significant influence on the ultimate bearing capacity. In this simulation, the extended Drucker-Prager elasto-plastic constitutive model (extended D-P model) is used to simulate the elasto-plastic behavior of the sediments. The yield criterion of extended Drucker-Prager model is written as

$$t - p\tan\beta - d = 0 \tag{3}$$

where t is the deviatoric stress measure defined as

$$t = \frac{q}{2}\left[1 + \frac{1}{K} - \left(1 - \frac{1}{K}\right)\left(\frac{R}{q}\right)^3\right] \tag{4}$$

in which β is the slope of the linear yield surface in the p–t stress plane; p is the equivalent pressure stress; R is the third invariant of deviatoric stress; q is the Mises equivalent stress; d is the cohesion of the material; K is the ratio of the yield stress in triaxial tension to the yield stress in triaxial compression. The extended D-P model is preferable to reflect the granular-like property of frictional materials and exhibit pressure-dependent yield. The extended D-P model gives a good approximation to Mohr-Coulomb model, the relationship of these parameters in the two constitutive models are as follows [16]: $\tan\beta = \sqrt{3}\sin\phi$; $d = \sqrt{3}\cos\phi \cdot c$, where ϕ is the angle of internal friction of soil, c is the cohesive strength of soil. The extended D-P model defines the yield surface as being a circle in the deviatoric π plane while for Mohr-Coulomb model it's a hexagon; this will benefit the convergence of the iterative algorithm.

2.3. Boundary conditions

As illustrated in Fig. 1(b), the top side of the mode is treated as a free boundary. The left side is an axisymmetric boundary, i.e. both the translational and rotational degrees of freedom in x direction are constrained to zero. At the right side of the model, the translational degree of freedom in x direction is constrained. At the bottom of the model, the translational degrees of freedom in both x and z directions are fixed.

The interfacial behavior is a key issue to efficiently simulate the complex tension pile-soil/rock interactions. In previous numerical works, the interfacial bonding mechanism and sliding friction mechanism could only simulated individually; nevertheless they are actually in coupled actions.

In the present study, to order to simulate these two coupled mechanisms, we propose an updated contact-pair model from the existing contact-pair algorithm [16]. As illustrated in Fig. 2, the revised algorithm is defined in terms of two surfaces interacting with each other by an updated "contact pair". Thus, the interfacial constitutive relationships can be implemented by defining the contact constraint of combined contact-pairs. To this aim, a user-defined interfacial constitutive relationship is programmed with the user-written subroutines to supplement the existing contact-pair model library. Two contact states between the two material surfaces are defined (see Fig. 2). If the normal distance of a node to the other surface is less than a specified value (w_n), then the contact is closed and the interfacial constitutive takes action; otherwise, the contact is open and no constraint is applied to the contact-pair. For the contact pairs in the closed sate, the bonding effect and the friction effect will influence both the tangent and the normal directions:

- Tangent contact property:
  As shown in Fig. 3(a), the maximum tangent stress (τ_{max}) is the sum of the interfacial bonding strength (c_i) and the frictional shearing stress ($\sigma_n \tan\delta$), i.e. $\tau_{\max} = c_i + \sigma_n \tan\delta$, where σ_n is the interfacial normal stress; δ is the friction angle of the pile-soil interface. The bonding breaks if the relative sliding distance is larger than a specified value w_t, and the interfacial tangent stress degrades into the pure frictional shearing stress: τ_{res}-$\sigma_n tan\delta$.
- Normal contact property:
  As shown in Fig. 3(b), the bonded surfaces have the ability to resist certain external tensile force. The maximum normal tensile stress is equal to the bonding strength. When the external tensile force exceeds the interfacial resistance, the breakage of bonding occurs and interfacial normal stress tends to decrease. The contact surface gets into the open state when the interfacial normal stress decreases to zero.

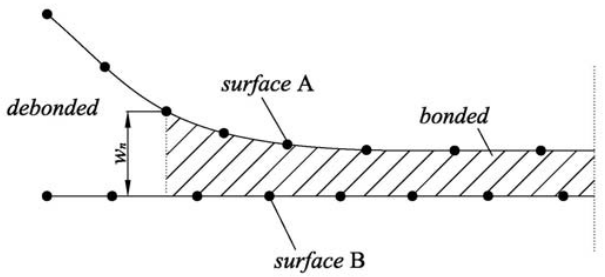

Fig. 2. Two contact states of interfacial surfaces in the updated contact-pair algorithm

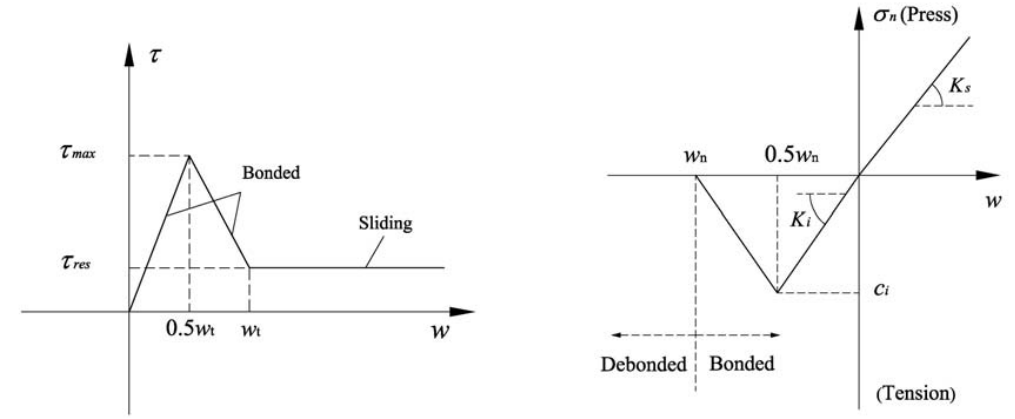

(a) (b)

Fig. 3. Proposed interfacial constitutive relationships for the updated contact-pair algorithm: (a) Tangential shear stress; (b) Normal stress

2.4. *Verification with experimental results*

To verify the proposed finite element model, comparisons are made between the present numerical results and two series of existing experimental results (see Fig. 4), i.e. the tension-pile tests in sands by Sowa [17]; and the tests of rock-bored tension-piles by He [18].

For the tension-pile embedded in sands, the calculated bearing tension loads for only considering the friction mechanism is in good agreement with the experimental data (see Fig. 4(a)). For the tension-pile embedded in the rock, the pure frictional resistance is significantly lower than the total bearing capacity; nevertheless, the results of the numerical model for considering the combination of bonding and sliding friction mechanisms match quite well the experimental results (see Fig. 4(b)). This indicates that the present finite element model including the updated contact-pair algorithm is capable of simulating both the interfacial bonding and sliding friction mechanism.

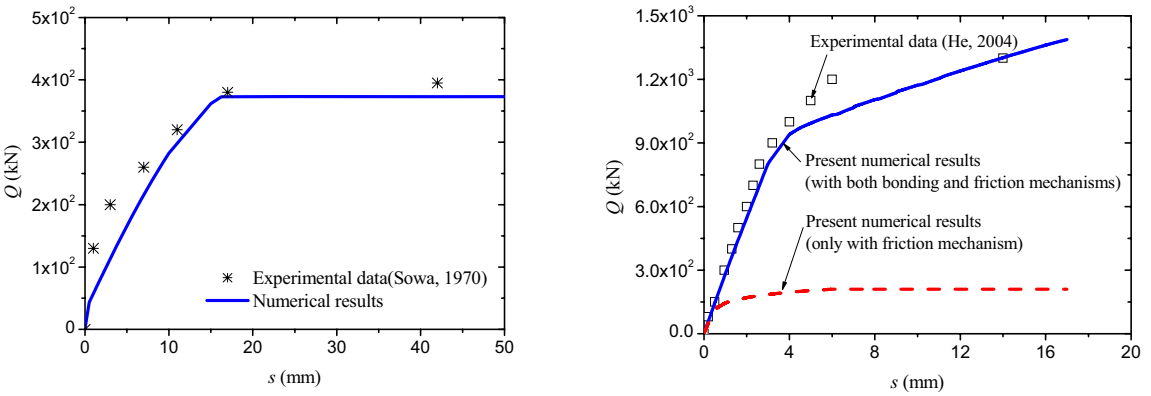

(a) (b)

Fig. 4. Comparisons between the present numerical results and the existing experimental results of (a) tests in sands by Sowa [17] (D=0.38m, L=12.00m); and (b) tests in rock by He [18] (D=0.6m, L=18.4m)

3. Numerical results and discussions

As aforementioned, the proposed FEM model may be used for simulating both interfacial bonding effect and friction effect on the uplift resistance of the tension pile embedded in various types of sediments, such as sand, clay and rock. The parameters for the examined pile and sediments are listed in Table 1.

Table 1. The parameters for the tension pile and sediments

	Pile length L (m)	Pile diameter D (m)	Mass density ρ (kg/m^3)	Young's modulus E (GPa)	Poisson's ratio ν	Cohesion strength c (kPa)	Angle of internal friction ϕ (^{0})	Factor of pile-soil friction $\tan\delta$
Pile	10.0	1.0	2.3×10^3	28.0	0.17	/	/	/
Sample 1: Sand	/	/	1.8×10^3	0.015	0.35	0.1	30	0.58
Sample 2: Clay	/	/	1.8×10^3	0.30	0.25	80	20	0.36
Sample 3: Rock	/	/	2.1×10^3	20.0	0.20	1.5×10^3	45	1.00

3.1. Interfacial bonding effects on bearing capacity of tension piles embedded in various sediments

The numerical results on the effects of interfacial bonding strength (c_i) on the bearing capacity of tension piles are shown in Fig. 5(a). In this figure, Q_p represents the bearing capacity taking into account of both bonding and friction effects; Q_{p0} is the tension capacity for which only the friction effect is considered.

With the increase of interfacial bonding strength, the trends for the variation of bearing capacity with bonding strength differ markedly for various kinds of sediments. For the pile in sands, the tension bearing capacity changes slightly with increasing interfacial bonding strength. But for the piles in clay or rock, a remarkable increase of bearing capacity is induced with the increase of bonding strength. Due to the bonding effect, the enhancement of the tension bearing capacity gets more obvious when the strength of sediment gets higher. Note that if the interfacial bonding strength is beyond a critical value $c_i/c \geq 1.0$, i.e. the interfacial bonding strength gets larger than soil cohesion strength, the bearing capacity of tension pile would stop growing (see Fig. 5(a)).

3.2. Effects of pile length on pile bearing capacity in sands

To examine the effects of pile length on the tension capacity, the tension piles with various values of embedded length in sand and rock under axial tension load are numerically modeled. As discussed above, the interfacial friction is the primary component of the tension capacity for the pile embedded in sands. Quite a few empirical approaches have already been proposed to calculate the bearing capacity of tension piles only taking into account the interfacial friction mechanism. The pile-soil sliding resistance mobilized by friction mechanism is written as $\tau_i = \sigma_n \tan\delta$, then the tension bearing capacity is derived as

$$Q_p = \frac{\pi}{2} DK' \gamma L^2 \tan\delta \tag{5}$$

which is the conventional standard empirical model to evaluate the bearing capacity of tension piles in the sands, where K' is the lateral pressure coefficient, γ is the unit weight of sediment (the buoyant unit weight for under water conditions). Fig. 5(b) gives the comparisons of the variation of the tension capacity with the pile embedment depth between the numerical results and the empirical standard model. In this case, only friction mechanism is considered in the numerical model. As the pile length increasing, both the contact area and the sliding resistance keep growing, thus the tension capacity of long pile in sands increases dramatically.

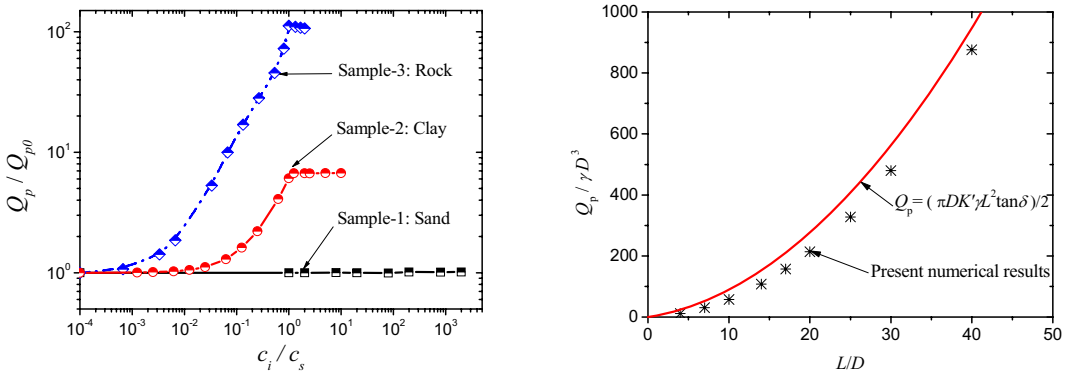

(a) (b)

Fig. 5. (a) Bonding effect on tension capacity of tension piles (D=1.0m, L=10.0m); (b) Comparison between numerical and empirical results for pile in sand (D=1.0m, γ =1.8×10^3 N/m^3, K'=0.54, $\tan\delta$ =0.58)

3.3. *Interfacial shear degradation effects: Critical embedded length*

The uplift bearing capacity of tension pile foundation usually increases with the increase of pile length; nevertheless, for the long slender piles, the uplift bearing capacity may stop growing with increasing pile embedment length. This phenomenon called "critical embedded length" has been noticed in some field tests.

Fig. 6 gives the variation of the dimensionless bearing capacity with the pile embedment-to-length ratio for the rocks with various values of Young's modulus (E_s). Both the friction mechanism and bonding mechanism are taken into account in this simulation. Compared with the tension pile in sands (see Fig. 5(b)), the bearing capacity of the tension pile in rocks tends to increase gradually to a constant for the long piles (see Fig. 6).

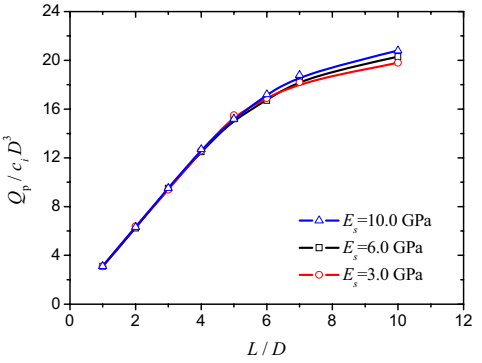

Fig. 6. Variation of tension capacity with pile slenderness ratio for various values of Young's modulus of rocks (D=1.0m, γ =2.06×10^3 N/m^3, c_s =1.5MPa, ϕ =45^0, c_i =250kPa, $\tan\delta$ =1.0)

The major difference between the piles embedded in sands and in rocks is whether or not the interfacial bonding takes effect. The degradation of bonding effect is the main reason for the "critical embedded length" phenomenon. The degradation of bonding effect is often found in piles or metal bolts socketed in rock, while it gets much slighter in the soft clay or sand. For the validation purpose, the distribution of interfacial sliding displacement and the shear stress along the pile depth are illustrated in Fig. 7 (a) and (b), respectively.

As shown in Fig. 7(a), the interfacial slide distance develops from the pile-top to the pile-bottom with increasing uplift loads. Due to the breakage of the bonding mechanism, the degradation of shear stress occurs firstly at the pile-top and then spreads to the pile-bottom. Fig. 7(b) indicates that the interfacial shear stress drops down obviously where the bonding degradation phenomenon takes place. Consequently, the interfacial shear stress are always mobilized only within certain part along the whole pile, especially for a long tension pile; while in the left parts of the pile, the shear stress is ignorable due to the bonding degradation.

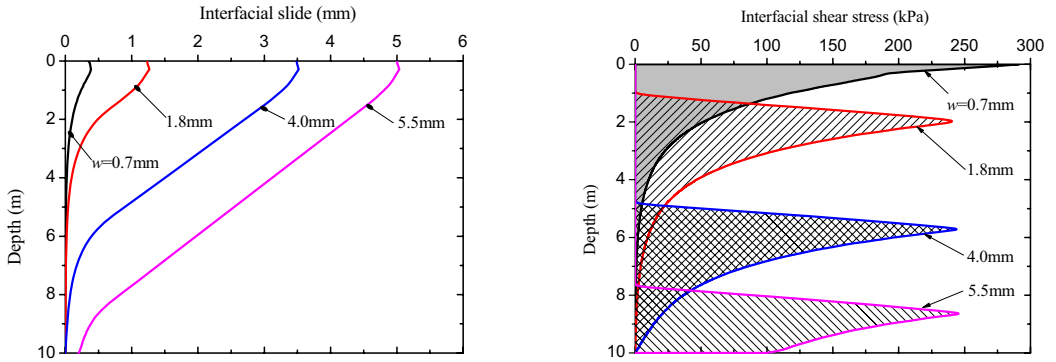

(a) (b)

Fig. 7. (a) Distribution of interfacial slide along the pile; (b) Distribution of interfacial shear stress along the pile (D=1.0m, L=10.0m, γ =2.06×10^3 N/m^3, c_s =1.5MPa, ϕ =45^0, c_i =250kPa, $\tan\delta$ =1.0)

4. Conclusions

The pile-soil interfacial behavior is a key issue for efficiently evaluating the bearing capacity of tension piles installed in various sediments in the field. To simulate the complex interaction between a single tension-pile with the neighboring sediments, a two-dimensional axisymmetric finite element model is proposed and verified with the existing experiments. Both the interfacial bonding mechanism and sliding friction mechanism are fulfilled in the present FEM with an updated contact-pair algorithm.

The interfacial bonding effects on bearing capacity of tension piles in various sediments are examined with the proposed numerical model. The enhancement of the tension bearing capacity gets more obvious when the cohesion strength of sediment gets higher. Interfacial shear degradation effects are investigated to reveal the mechanism of the “critical embedded length” phenomenon, which was previously noticed in the engineering applications. The distributions of interfacial sliding displacement and the shear stress along the pile depth indicate that, the degradation of shear stress occurs firstly at the pile-top and then spreads to the pile-bottom due to the breakage of the bonding mechanism; meanwhile, the interfacial shear stress are always mobilized only within certain part along the whole pile, especially for a long tension pile. The interfacial bonding degradation of is the main reason for the occurrence of “critical embedded length” phenomenon.

Acknowledgements

Financial support by the Knowledge Innovation Program of the Chinese Academy of Sciences (Grant no. KJCX2-YW-L07) is greatly appreciated.

References

[1] Randolph MF. Science and empiricism in pile foundation design. *Geotechnique* 2003; 53(10): 847-875.

[2] Meyerhof GG, Adams J I. The ultimate uplift capacity of foundations. *Canadian Geotechnical Journal* 1968; 5(44): 225-244.

[3] Das BM. A procedure for estimation of uplift capacity of rough piles. *Soils and Foundations* 1983; 23(3):122–126.

[4] Chattopadhyay BC, Pise PJ. Uplift capacity of piles in sand. *Journal of Geotechnical Engineering* 1986; 112(9): 888-904.

[5] Thorne CP. The allowable loadings of foundations on shale and sandstone in the Sydney region. Part 3: Field tests results. *Sydney Group of Australian Geomechanics Society, Institute of Engineers of Australia*. 1977.

[6] Poulos HG, Davis EH. *Pile Foundation Analysis and Design*. New York: Wiley; 1980.

[7] Hooley P, Lefroy SR. The ultimate shaft frictional resistance mobilised by bored piles in over-consolidated clays and socketed into weak and weathered rock. In: Cripps JC et al., editors. *The Engineering Geology of Weak Rock*. Rotterdam: Balkema, 1993; p. 447-55

[8] Liu ZD. Foundation of tension piles. *Ground Improvement* 1995; 6(4): 1-12.

[9] Cai Y, Esaki Y, Jiang Y. A rock bolt and rock mass interaction model. *International Journal of Rock Mechanics & Mining Sciences* 2004; 41: 1055-1067.

[10] Gu XF, Haberfield CM. Laboratory investigation of shaft resistance for piles socketed in basalt. *International Journal of Rock Mechanics & Mining Sciences* 2004; 41(3): 1-6.

[11] Costamagna R, Renner J, Bruhns OT. Relationship between fracture and friction for brittle rocks. *Mechanics of Materials* 2007; 39: 291-301.

[12] Rowe RK, Pells PJN. A theoretical study of pile-rock socket behaviour. *International Conference on Structural Foundations on rock,* Sydney; 1980.

[13] Cai Y, Esaki T, Jiang Y. An analytical model to predict axial load in grouted rock bolt for soft rock tunneling. *Tunnelling and Underground Space Technology* 2004; 19: 607-618.

[14] Xiao SJ, Chen CF. Mechanical mechanism analysis of tension type anchor based on shear displacement method. *J. Cent. South Univ. Technol.*, 2008; 15: 106-111.

[15] He SM, Wu Y, Li XP. Research on mechanism of uplift rock-socketed piles. *Rock and Soil Mechanics* 2009; 30(2): 333-344.

[16] Hibbitt, Karlsson and Sorenson Inc. *ABAQUS Theory Manual*, Version6.8-1. 2008.

[17] Sowa VA. Pulling capacity of concrete cast in situ bored piles. *Canadian Geotechnical Journal* 1970; 7: 482-493.

[18] He J. Testing study on anti-draw bearing properties of cast-in-place rock-socked pile. *Chinese Journal of Rock Mechanics and Engineering* 2004; 23(2): 315-319.